Lipid biomarker (brGDGT)- and pollen-based reconstruction of temperature change during the Middle to Late Holocene transition in the Carpathians

Ramos-Roman, Maria J.

2022-08

Lipid biomarker (brGDGT)- and pollen-based reconstruction of temperature change during the Middle to Late Holocene transition in the Carpathians

María J. Ramos-Román [a,*], Cindy De Jonge [b], Eniko Magyari [c], Daniel Veres [d], Liisa Ilvonen [e], Anne-Lise Develle [f], Heikki Seppä [a]

[a] Department of Geography and Geosciences, Faculty of Science, University of Helsinki, Helsinki, Finland
[b] ETH Zürich, Geological Institute, 8092 Zürich, Switzerland
[c] MTA-MTM-ELTE Research Group for Paleontology, Department of Environmental and Landscape Geography, Eötvös Loránd University, Pázmány Péter stny. 1/C, 1117 Budapest, Hungary
[d] Institute of Speleology, Romanian Academy, Clinicilor 5, 400006 Cluj-Napoca, Romania
[e] Organismal an Evolutionary Biology Research Program, Research Centre for Ecological Change, University of Helsinki, Finland
[f] Université Grenoble Alpes, Université Savoie Mont Blanc, CNRS, EDYTEM, Le Bourget du Lac, France

ARTICLE INFO

ABSTRACT

To reconstruct changes in vegetation, temperature, and sediment geochemistry through the last 6.5 cal ka BP, in the Subcarpathian belt of the Eastern Carpathians (Romania), pollen, branched glycerol dialkyl glycerol tetraethers (brGDGTs) and X-ray fluorescence analyses have been integrated. Pollen and brGDGTs (a bacterial lipid biomarker proxy) are used as paleothermometers for reconstructing the mean annual air temperature (MAAT) and mean temperature above freezing (MAF), respectively. Both proxies show roughly consistent records. The highest MAAT and MAF occurs during the oldest part of the record (from 6.5 to 4.2 cal ka BP), and the Middle to the Late Holocene shift is marked by a prominent decrease in temperature between 5.4 and 4.2 cal ka BP, coinciding with Bond event 4 and 3. This transition is coeval with a decrease in summer insolation, shift from consistent NAO- conditions to a predominance of NAO+ phase and coincides with the beginning of the Neoglacial cooling in northern latitudes. The warm bias in the MAF reconstruction during the Late Holocene is explained as a change in the lipid provenance or in the composition of the brGDGT producers after 4.2 cal ka BP.

1. Introduction

The Middle- to Late Holocene transition, coinciding with the end of the Holocene Thermal Maximum (HTM) and the beginning of the Neoglacial cooling in northern latitudes (~5.8–5 cal ka BP), has been the focus of paleoclimate studies during the last decades. A decreasing trend in temperature towards the Late Holocene has been suggested by different paleoclimate reconstructions in the North Atlantic area (Rasmussen et al., 2016) showing a pronounced cooling (i.e., a decrease in mean annual temperature up to 3 °C) (Magyari et al., 2013; Moossen et al., 2015; Tóth et al., 2015; Martin et al., 2020). However, some controversy remains on the temperature response during the Middle-Late Holocene reflecting, i) regional discrepancies among different datasets (Kaufman et al., 2004; Peyron et al., 2011; Fohlmeister et al., 2012; Baker et al., 2017; Perşoiu et al., 2017;), and ii) difference in the seasonality of the temperature reconstruction (Fohlmeister et al., 2012;

Drăguşin et al., 2014; Moossen et al., 2015; Perşoiu et al., 2017; Baker et al., 2017). This point of chronological and data inconsistence in the occurrence of this cooling has been denoted in other studies (Orme et al., 2021). It suggests either actual lack of regional synchronicity in past climate variability modulated by a strong and as yet not-well assessed interaction of the Atlantic, Mediterranean and Siberian High pressure systems that seasonally affect the East-Central Europe (see discussion in Haliuc et al., 2017; Longman et al., 2019), and/or uncertainties in chronological data. In the Carpathian area, situated at the contact of these three major atmospheric circulation patterns, several recent studies have discussed Holocene paleoclimate dynamics in humidity and temperature (e.g. Tantau et al., 2006; Feurdean et al., 2008; Drăguşin et al., 2014; Tóth et al., 2015; Feurdean et al., 2015; Perşoiu et al., 2017; Longman et al., 2017a, 2017b; Haliuc et al., 2017; Magyari et al., 2018). However, because of the lack of reliable quantitative temperature reconstructions during the Middle to Late Holocene transition, there is a

---

need for additional higher-resolution studies based on more refined and accurate quantitative reconstruction methods.

To examine the climate history of the Middle and Late Holocene in the Carpathian area, we present a high-resolution paleotemperature record from Lake Mocearu located in the Subcarpathian range (Fig. 1). A sediment core (Moc-02) was collected that records the last 6.5 cal ka BP, including the transition from the Middle to Late Holocene. Branched glycerol dialkyl glycerol tetraethers (brGDGTs) and pollen based quantitative temperatures are reported. To constrain the provenance of the brGDGTs, we analyzed these in catchment soil and suspended particulate material (SPM) from the lake water column.

BrGDGTs have been used recently as novel paleothermometers providing temperature reconstructions in marine and lacustrine sediment cores (e.g. Weijers et al., 2007; Moossen et al., 2015; Martin et al., 2019, 2020). These compounds are a family of bacterial membrane-spanning lipids consisting of two alkyl chains ether-bound to glycerol molecules. The structural diversity of the lipids used as paleoclimate proxies is caused by the changing numbers of methyl branches (4–6) and cyclopentane moieties (0–2) incorporated in the two alkyl chains (Sinninghe Damsté et al., 2000; Weijers et al., 2006). Furthermore, the outer methyl branch(es) can be located on C5 (5-methyl brGDGT) or C6 (6-methyl brGDGT) position of the alkyl chain (De Jonge et al., 2013). Variation in the methylation of 5-methyl brGDGTs is summarized as the MBT'$_{5ME}$ ratio (De Jonge et al., 2014). In a set of globally distributed lakes, the MBT'$_{5ME}$ ratio reveals a strong temperature dependency, which is the basis of the temperature calibration developed by Martínez-Sosa et al. (2021) and Raberg et al. (2021). While temperature is the main driver of the paleotemperature proxy on the global scale, bacterial community changes have been shown to influence this ratio in lakes (Weber et al., 2018) and soils (De Jonge et al., 2019; De Jonge et al., 2021). Although brGDGTs encountered in surface lake sediments are interpreted to be dominantly derived from lacustrine bacteria (Tierney and Russell, 2009; Martínez-Sosa et al., 2021), a possible contribution of soil-derived lipids cannot be excluded and has been encountered in Holocene lake settings previously (Martin et al., 2020).

Fossil pollen have been used in paleoecological and paleoclimatic reconstructions for many decades (Birks et al., 1990). The quantitative reconstruction from fossil pollen assemblages is based on a comparison with modern pollen assemblages and their associated modern climatic parameters. During the last decades pollen data have been used as a proxy for quantitative paleotemperature reconstructions using different transfer functions and training sets (Davis et al., 2003; Peyron et al., 2011; Juggins and Birks, 2012; Peyron et al., 2013, 2017; Tarroso et al.,

2016; Bini et al., 2019; Chevalier et al., 2020). Here we use the weighted average partial least squares (WAPLS) technique, as developed by ter Braak and Juggins (1993). A comparison is made between paleotemperature reconstructions based on pollen and brGDGTs, before the implication of the temperature variation on the regional climate system is discussed.

2. Geographical setting and sampling

2.1. Geographical setting

The study area is located west of the Black Sea in the flysch and salt karst region of Buzau Subcarpathians (Fig. 1; Móga et al., 2018). The 2.9 km^2 Mocearu Plateau, situated at an altitude of 400–600 m a.s.l., has a quadrangular shape. The climate of the area is temperate continental (Fărcaş and Sorocovschi, 1992). Average annual rainfall is 650 mm, annual mean temperature is 10.7 °C, where mean July temperature is 21.6 °C and mean January temperature − 0.5 °C (interval 1991–2016; Strat, 2016). Snow cover duration is around 100 days at low altitudes in the Subcarpathians (Kern et al., 2004). Atmospheric circulation is dominated by cold and dry air masses coming from north/north-east (i. e., the Siberian High) during winter, whereas in summer western air masses predominate, alongside periodic input of Mediterranean and/or Black Sea derived moisture (Biagioni and Rapetti, 2005). The North Atlantic oscillation (NAO) is the main mechanism controlling precipitation and temperature variability in East-Central Europe, but with a strong modulation by the Siberian High especially during the winter months (Fărcaş and Sorocovschi, 1992). The westerlies associated with a negative NAO bring moisture from the North Atlantic and the Mediterranean Sea mainly during autumn and winter towards East-Central Europe (Fărcaş and Sorocovschi, 1992; Perşoiu et al., 2017). When the NAO is in a positive phase, the westerlies are displaced northward resulting in drier conditions in East-Central Europe (Bojariu and Paliu, 2001; Bartholy et al., 2009). The East-Central European climate patterns are strongly influenced by the dynamics of storm tracks from these systems (Bojariu and Paliu, 2001; Bartholy et al., 2009).

Lake Mocearu (45.46818 N; 26.55244 E; Fig. 1), located at 780 m a.s. l., has an area of 0.97 km^2, and a small catchment area (5.88 km^2; Fig. 1). The mean annual temperature at Lake Mocearu is 7.3 °C (WorldClim; Fick and Hijmans, 2017). The vegetation in the watershed is dominated by trees such as, *Betula pendula, Pinus sylvestris, Alnus glutinosa, Abies alba, Fagus sylvatica, Picea abies, Populus tremula, Carpinus betulus, Tilia cordata, Acer platanoides*, and shrubs such as *Crataegus*
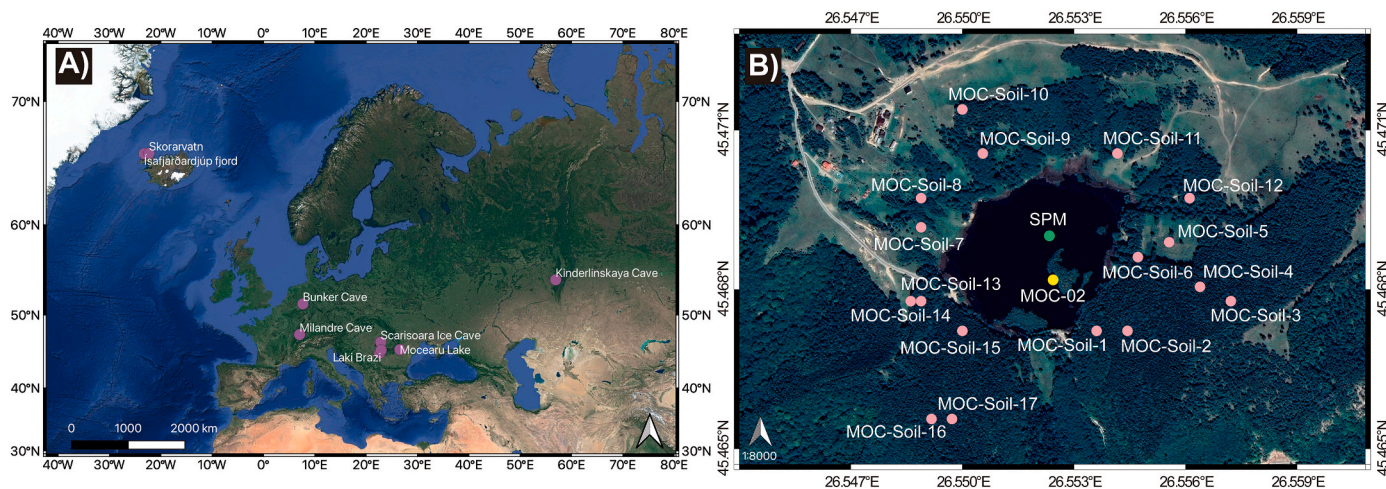
Fig. 1. A) Location of the Mocearu lake in the east central Europe and other northern hemisphere records use in this study. B) Location of the downcore Moc-02 (yellow point), soil samples on the watershed (pink points) and suspended particulate material (SPM) (green point) on the Mocearu lake (Buzau County, Romania). (For interpretation of the references to colour in this figure legend, the reader is referred to the web version of this article.)

monogyna and herbs predominantly *Festuca* and *Poa* sp. Pine (*P. sylvestris*) plantations are common in the area. Shoreline vegetation is characterized by emergent aquatic plants belonging to Cyperaceae and *Typha latifolia* (Supplementary Table S1).

2.2. Sampling

In August 2019 using a Livingstone corer operated from a platform placed on rubber boats two sediment cores were recovered with a length of 100 cm (Moc-01) and 600 cm (Moc-02), respectively. The cores were stored in darkness, at +4 °C at the Eötvös Loránd University (Budapest, Hungary). Furthermore, eighteen soil samples were taken at Lake Mocearu, around the catchment at different distances from the lake shore. To collect suspended particulate matter in the lake water column, a sample (2 l) was collected at 1 m below lake surface and subsequently filtered using a 0.45 μm (pore size) cellulose nitrate filter (Fig. 1). The description of the vegetation present at the soil sample sites is reported (Supplementary; Table S1).

3. Materials and methods

3.1. Chronology

The age-depth model of the Moc-02 core was calculated using a Bayesian age-depth modelling in R-package (RStudio Version 1.3.1093; R Development Core Team, 2015) `BACON' (Blaauw and Christen, 2011). The age-depth model is based on 12 AMS radiocarbon dates, a total of 11 samples have been analyzed from wood material (Table 1). The Bayesian age-depth model was built using the calibration curve IntCal 20 (Reimer et al., 2020). The parameters of the model are included in Fig. 2. Sediment accumulation rate (SAR) have been estimated from the Bayesian age-depth model. In the discussion, we follow the subdivision of the Holocene by Walker et al. (2012), with the Middle-to Late Holocene transition at 4.2 cal kyr BP.
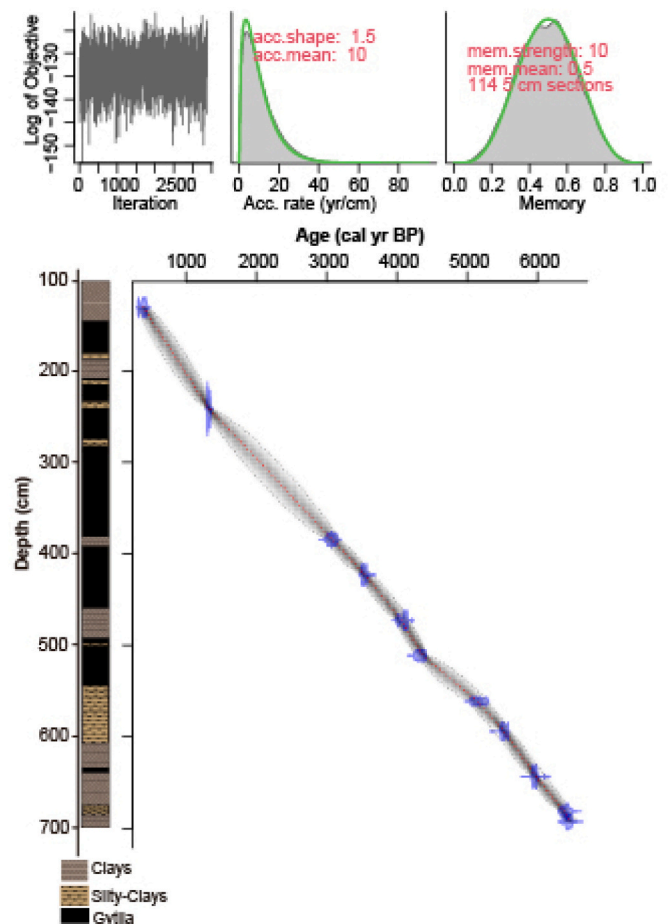
3.2. Lithology; loss-on-ignition and XRF analysis

The Moc-02 core sections were split longitudinally and visual changes in lithology were described using the Troels-Smith sediment description system (Fig. 2). The total organic matter content (LOI$_{550}$) of 89 samples was analyzed by loss on ignition (LOI) (Dean, 1974; Heiri et al., 2001). Measurements were made with an automated thermogravimetric analyzer (TAG) that dried and heated the sample at 550 °C until they reached mass constancy. Elemental geochemical composition was measured with an X-ray fluoresce (XRF) Avaatech Core Scanner at the EDYTEM (France). Measurements were taken contiguously at 0.5 cm spacing resolution. A total of 20 chemical elements were measured with the XRF core scanner using 10 s count time, 10 kV X-ray voltage, and X-ray current of 90 μA for lighter elements and a 20s count time, 30 kV X-
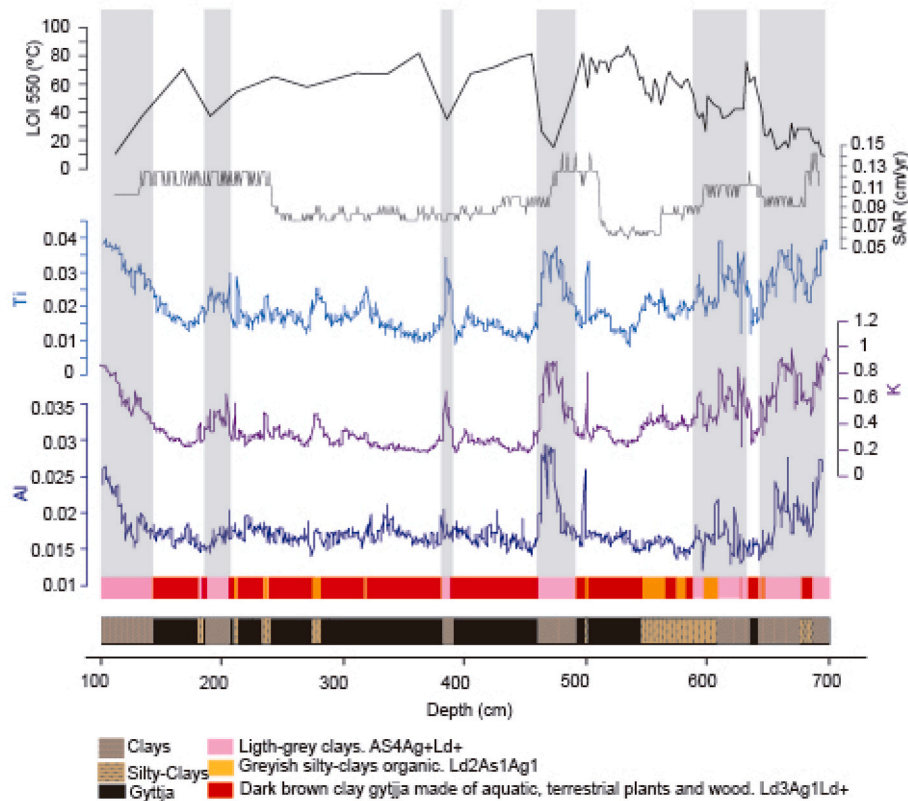

Fig. 2. Bayesian age-depth model of the Moc-02 record for the last 6500 cal yr BP. See Tables 1 for specific information about the radiocarbon samples. Acronyms: acc. Shape, accumulation shape; acc. Mean, accumulation mean, mem. Strength, memory strength; mem. Mean, memory mean.

ray voltage, and X-ray current of 150 μA for heavier elements. Here we use only K, Al, and Ti as the most representative elements associated with terrestrial input (Kylander et al., 2011) (Fig. 3). Results are presented as normalized data, calculated as the counts per second (cps) of every element divided by the sum of the total counts (cps). This normalization is applied to reduce the effect of the sediment density, water content, and/or the core surface conditions (Bahr et al., 2014).

3.3. Pollen analysis and quantitative reconstructions

A total of 61 samples (1 cm^3) for pollen analysis were taken throughout the core (with 250 yr resolution between 4 and 0.2 cal ka BP and 60 yr resolution from 6.5 to 4 cal ka BP). Pollen extraction followed established methods (Faegri and Iversen, 1989). Processing included the addition of *Lycopodium* spores. Sediment samples were treated with NaOH, HCl, and HF and the residue was sieved at 250 μm prior to acetolysis. Counting was done using a transmitted light microscope at 400 magnifications to an average of 340 terrestrial pollen grains. Fossil pollen was identified using published keys (Beug, 2004). The pollen diagram was made using R (RStudio Version 1.3.1093; R Development Core Team, 2015) package 'Rioja'. Percentage of all pollen taxa were calculated based on the summed terrestrial pollen, excluding aquatic plants (Supplementary Fig. S2). The zonation of the pollen taxa was made using stratigraphically constrained cluster analysis (CONISS) to identify the different climatic subdivisions. This includes the transition from Middle to Late Holocene and shorter climatic events within this

Table 1
Age data for Moc-02 record. All ages were calibrated using R-code package 'BACON' employing the calibration curve IntelCal 20 (Reimer et al., 2020) at 95% of confidence range.

| Laboratory number	Core	Material	Depth (cm)	Age (14C BP ± 1σ)	Median age (cal yr BP)
BRAMS_3595	MOC_02_1_525	Wood	130.9	316 ± 13	391
BRAMS_3596	MOC_02_2_634	Wood	241.81	1412 ± 18	1314
BRAMS_3597	MOC_02_3_771	Wood	384.42	2921 ± 14	3066
BRAMS_3598	MOC_02_4_820	Wood	423.05	3330 ± 15	3528
BRAMS_3599	MOC_02_5_820	Wood	472.8	3740 ± 15	4103
BRAMS_3600	MOC_02_5_910	Wood	511.26	3885 ± 15	4334
BRAMS_3601	MOC_02_5_950	Wood	561.32	4495 ± 16	5166
BRAMS_3602	MOC_02_6_976	Wood	593.99	4783 ± 21	5523
BRAMS_3603	MOC_02_6_1036	Wood	643.53	5205 ± 22	5964
BETA_537692	MOC_02_6_1067	Wood	681.68	5630 ± 30	6406
BETA_537690	MOC_02_6_1076	Wood	692.81	5660 ± 30	6438

Fig. 3. Moc-02 lithology, sediment accumulation rate (SAR), Loos on ignition (LOI) and XRF data. XRF data are presented as normalized data. Grey shadows represent low LOI values and high K, Al, and Ti values.

period (Supplementary Fig. S1).

We use weighted averaging partial least squares regression and calibration (WAPLS) as the quantitate method to reconstruct past mean annual air temperature (MAAT) (Fig. 4). A total of 8479 modern samples from the European Modern Pollen Database (Davis et al., 2020) were used to calculate the transfer function (Supplementary; Fig. S2). The transfer function method was used on a total of 244 pollen taxa. The actual annual mean temperatures were obtained using WorldClim in a 30-s resolution ($\sim$ 1 km^2) and represent average values for 1970–2000 time period (Fick and Hijmans, 2017). WAPLS is a non-linear, unimodal regression and calibration technique used in quantitative re-constructions (Juggins and Birks, 2012). We used a two-component WAPLS model and the pollen values were square root transformed for WAPLS regression to reduce noise in the data. The performance of the transfer function was evaluated by leave-one-out cross-validation (Birks et al., 1990). Based on the leave-one-out cross-validation results we calculated the coefficient of determination (r^2), root-mean-square error of prediction (RMSEP) and maximum bias as performance statistics (Supplementary Fig. S3; Table S2). Calculation of WAPLS transfer functions was performed in R (RStudio Version 1.3.1093; R Development Core, 2015) package 'Rioja' (Juggins, 2009).

3.4. BrGDGT analysis

A total of 115 sediment samples were analyzed for brGDGT analysis including 96 samples from the cores (with 250 yr resolution between 4 and 0.2 cal ka BP and 30 yr resolution from 6.5 to 4 cal ka BP), 18 soil samples from the catchment, and one filtered SPM sample from the lake surface waters. 1 cm^3 of sediments and soil were freeze-dried and homogenized, and the total lipid extracted using an automated solvent extraction system (EDGE) with dichloromethane (DCM): methanol (MeOH) (80:20, v:v). To obtain the total lipid of the SPM, the filter was
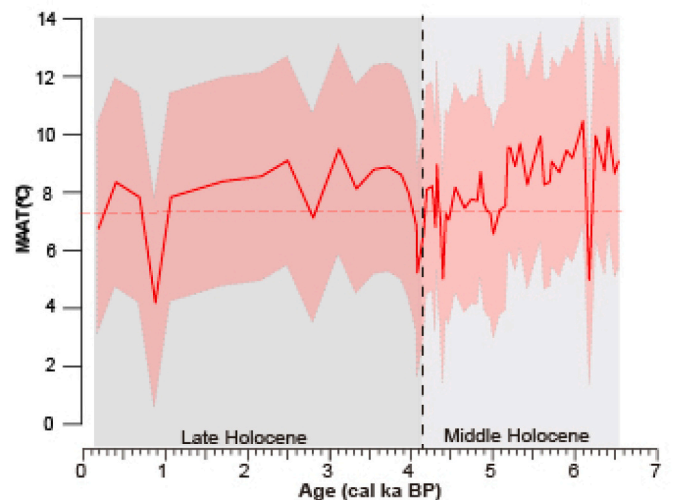
Fig. 4. Mean annual air temperature (MAAT) for the Moc-02 record based on pollen data and using WAPLS. The red shadow displays the standard error of the reconstruction. Dark grey and light grey shadings indicate the formal strati-graphical subdivision of the Holocene (Walker et al., 2012). (For interpretation of the references to colour in this figure legend, the reader is referred to the web version of this article.)

hydrolyzed by adding 4 ml of 1.5 N HCl in MeOH, leaving to react at 80 °C for 2 h. After bringing to more neutral pH (4–5) by adding 2 N KOH in MeOH, 4 ml of DCM and MilliQ water was added to induce phase separation. The lower phase was transferred and dried under a nitrogen stream. The total lipid extracted was separated over column with activated Al$_2$O$_3$ using hexane:DCM (9:1), hexane:DCM (1:1) and DCM:

MeOH (1:1) as eluents to isolate the apolar, keto and polar fractions, respectively. Before the Al_2O_3 separation, the internal standard C_{46} GDGT (Huguet et al., 2006) were added to the total lipid extracted. The polar fractions of these samples were filtered using a 0.45 μm PTFE filter, prior to the determination of the core lipid brGDGTs by atmospheric pressure chemical ionization/high performance liquid chromatography–mass spectrometry (HPLC-MS), using the configuration as describe by Hopmans et al. (2016), with a modified column temperature (40 °C). The different GDGT isomers were measured using selective ion monitoring (SIM) mode with m/z 1050, 1048, 1046, 1036, 1034, 1032, 1022, 1020, 1018, and 744. Peak areas were integrated manually.
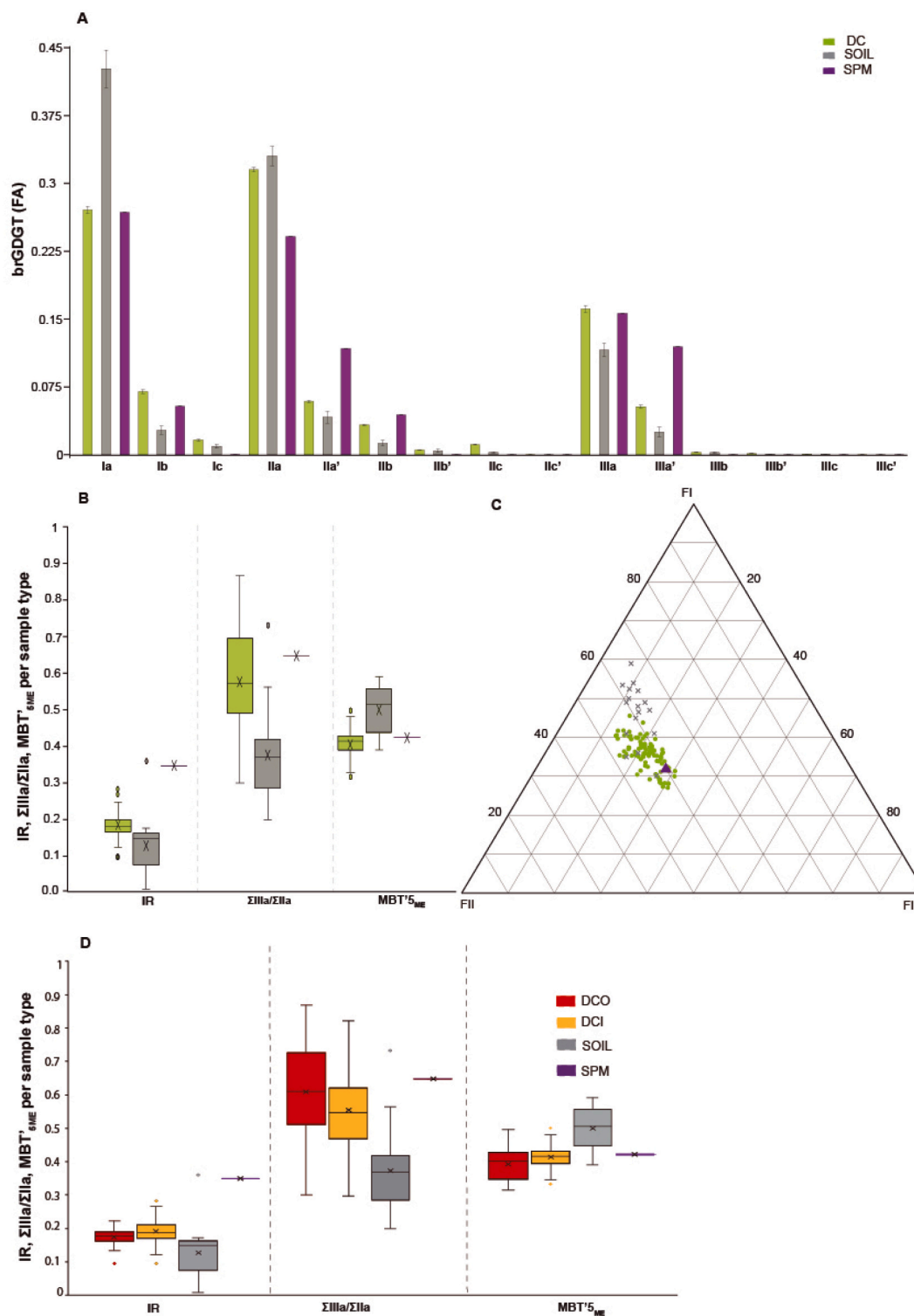
Fig. 5. A) BrGDGT fractional abundances (FA) per sample type. B) Comparison of boxplot of the MBT'$_{5ME}$, the IR and the ΣIIIa/ΣIIa ratio based on the relative abundance of the brGDGTs in the different sample types: DC (downcore), soil and SPM (suspended particulate material). C) Ternary diagram with the relative abundances of the tetramethylated (FI), pentamethylated (FII) and hexamethylated (FIII) compounds. D) Comparison of boxplot of the MBT'$_{5ME}$ based on the relative abundance of the brGDGTs in the different sample types: DCO (downcore organic facies), DCI (downcore clays facies) soil and SPM (suspended particulate material).

3.5. Calculation of brGDGTs-based indices and statistical analysis of the source of brGDGTs through time

Different calibrations have been developed to calculate MAAT and mean temperature of the month above freezing (MAF; mean temperature of the months with a mean temperature above 0 °C) based on the relative abundances of brGDGTs. The relative abundances are calculated as the proportion of each brGDGT compared to the total sum of all 15 brGDGT. The MBT'$_{5ME}$ index, that summarizes the variability in Methylation of 5-methyl Branched Tetraethers (De Jonge et al., 2014 [Eq.1]), has been calibrated against temperature in global lake systems (Martínez-Sosa et al., 2021; Raberg et al., 2021 [Eq.2]). To calculate MAAT and MAF, we tested the global lacustrine calibration by Raberg et al. (2021) ($n = 182$, $r^2 = 0.89$, RMSE = 2.32 °C), and the global Bayesian lacustrine calibration by Martínez-Sosa et al. (2021) ($n = 163$, $r^2 = 0.82$; RMSE = 2.9 °C), with a prior standard deviation (SD) set to 10 °C.

$$MBT'_{5ME} = ([Ia] + [Ib] + [Ic]) / ([Ia] + [Ib] + [Ic] + [IIa] + [IIb] + [IIc] + [IIIa]) \quad (1)$$

$$MAF \, (°C) = -0.5 + 30.4^* \, MBT'_{5ME} \quad (2)$$

To distinguish between brGDGTs sources and evaluate their response to environmental factors, relevant changes in the brGDGTs distribution are summarized as brGDGTs ratios (Figs. 5 and 6). We applied the isomer ratio (IR; Eq. 3) by (De Jonge et al., 2015), and the cyclisation of the branches tetraethers (CBT'; Eq. 4) by De Jonge et al. (2014), and the ΣIIIa/ΣIIa (Eq. 5) by Xiao et al. (2016). Xiao et al. (2016) combined the 5- and 6- methyl forms as in the 'traditional' chromatography technique, which did not separate the isomers (De Jonge et al., 2013); here we redefined the equation to explicitly include the 5 and 6-methyl compounds. To evaluate different dependencies between soil and lake brGDGTs, we plot the ratio of tetramethylated (Ia-Ic), pentamethylated (IIa-IIc) and hexamethylated (IIIa-IIIc) compounds using a triplot (Fig. 5). These ratios were calculated for the downcore, soil, and suspended particulate material (SPM) GDGT distribution (Fig. 5).

$$IR = ([IIa'] + [IIb'] + [IIc'] + [IIIa'] + [IIIb'] + [IIIc']) / ([IIa] + [IIa'] + [IIb] \\ + [IIb'] + [IIc] + [IIc'] + [IIIa] + [IIIa'] + [IIIb] + [IIIb'] + [IIIc] + [IIIc']) \quad (3)$$

$$CBT' = {}^{10}log \, (Ic + IIa' + IIb' + IIc' + IIIa' + IIIb' + IIIc') / (Ia + IIa + IIIa) \quad (4)$$

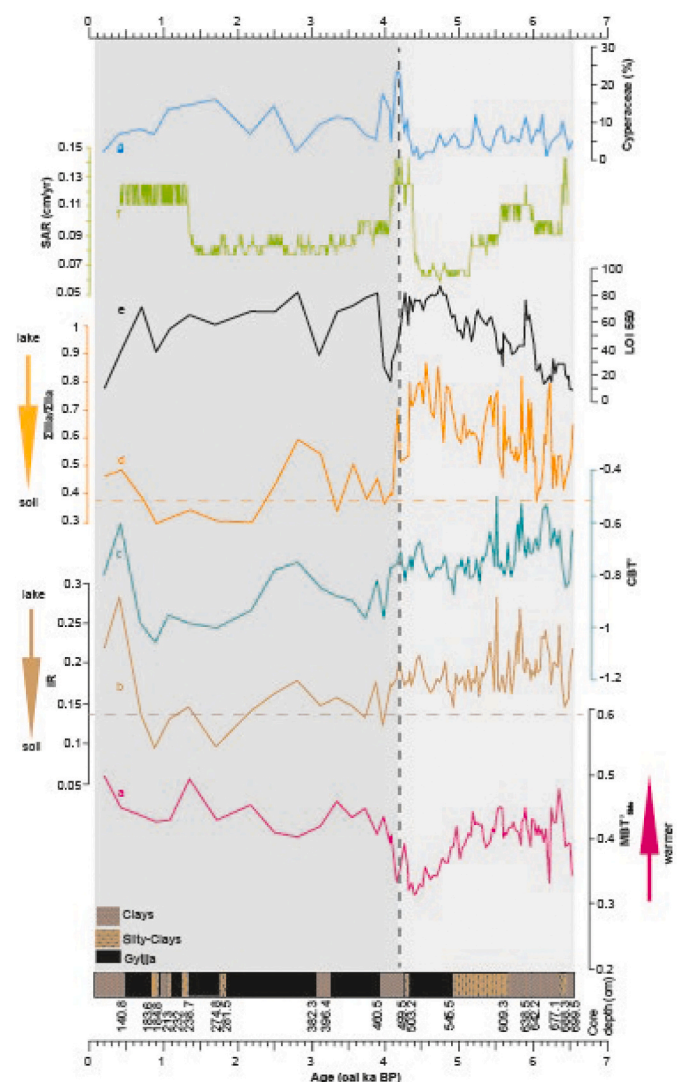$$ΣIIIa/ΣIIa = ([IIIa] + [IIIa'] + [IIIa'']) / ([IIa] + [IIa']) \quad (5)$$

4. Results

4.1. Chronology and sedimentary rates

The age-depth model shows that the sedimentary sequence covers the time interval from 6.5 cal ka BP to ~0.2 cal ka BP (Fig. 2). Sediment accumulation rate (SAR) varies between 0.06 and 0.14 cm/yr showing higher values from the bottom of the core to 591 cm (5.5 cal ka BP), 508 to 473 cm (4.3 to 4 cal ka BP) and 238 cm (1.3 cal ka BP) to the top of the core (Fig. 3).

4.2. Lithology and sedimentary facies

The lithology of core Moc-02 consists of alternation between organic (gyttja) and clastic (clays and silty-clays) intervals. The bottom of the core starts with clastic sediment until 590 cm (5.5 cal ka BP) associated with higher values of terrestrial elements [Al, K, and Ti; showing a high positive correlation between them (Ti-K = 0.96, Al-K = 0.57, K-Al = 0.52; $p < 0.05$)]. From 590 to 499 cm (5.4 to 4.3 cal ka BP) sediment

Fig. 6. BrGDGTs proxies, LOI, SAR and wetland pollen in Moc-02 record through the last 6.5 cal ka BP. a) MBT'5$_{ME}$ by De Jonge et al., 2014, b) IR by De Jonge et al., 2014, c) CBT' by De Jonge et al., 2014, d) ΣIIIa/ΣIIa ratio by Xiao et al., 2016, with the limit of aquatic dominion, e) LOI$_{550}$, f) SAR, g) Cyperaceae pollen percentage. Dark grey and light grey shadings indicate the formal stratigraphical subdivision of the Holocene (Walker et al., 2012).

consist mainly of gyttja, with some intercalations of silty-clays at 580, 570–560, and 500 cm. From 499 to 460 (4.2 to 3.9 cal ka BP) cm the sediment is composed of clays. After that, from 460 to 141 cm (3.9 to 0.5 cal ka BP) more organic-rich sediment dominates with some clays and silty-clay intercalations at 395–382, 281–275 and 213–184 cm depth. From 141 cm to the top of the core silty clays are the dominant component (Fig. 3).

The organic matter content (LOI$_{550}$) ranges from 87% in the organic-rich layers to 9.2% in clastic material, reaching their minimum values at the bottom of the record. A general increasing trend from the bottom to around 497 cm (4.2 cal ka BP) occurs, after those higher values of organic matter occurs interrupted by several relative minimums at 473 cm, 384, 189, and 111 cm (Fig. 3). LOI$_{550}$ shows a negative correlation with the terrestrial elements (Ti-LOI = −0.83; $p < 0.05$).

4.3. Pollen

Pollen of most representative taxa, with values higher than 1%, were plotted in a summary pollen diagram (Supplementary Fig. S1). The

pollen assemblages are dominated by *Alnus* and *Quercus* deciduous throughout the record, with mean values around 40% and 15%, respectively. The herbs and grasses such as *Artemisia* and Poaceae, and aquatic plants such as *Typha latifolia* are present through the record. The lakeshore emergent wetland plant group Cyperaceae (sedges) is also present throughout the record, but their values fluctuate and show an increasing trend during the Late Holocene. In addition to the *Alnus* and *Quercus* dominance, the vegetation between 6.5 and 5.4 cal ka BP is marked by the presence of *Ulmus, Tilia, Corylus, Carpinus betulus, Abies alba, Acer, Picea abies* and *Pinus*. A significant characteristic between 5.4 and 4.2 cal ka BP is the higher relative frequency of herbs such as Apiaceae, showing a peak at values of around 30%. Between 5.2 and 4 cal ka BP an increase in *Alnus* is detected, reaching values around 70%, coincidently with a decrease in *Tilia, Ulmus* and *Pinus*. The transition to the Late Holocene is mainly marked by the appearance of *Fagus sylvatica* and the disappearance of Apiaceae around 4.2 cal ka BP. This zone is also marked by an increase in *Pinus, Picea abies* and *Tilia* relative frequencies. Finally, a slight increase (showing values lower than 5%) in the presence of anthropogenic indicator herbs such as *Plantago major* type and *Plantago lanceolata* is detected from the Middle to Late Holocene transition, starting at around 4.2 cal ka BP.

The current mean annual temperature for the Lake Mocearu area is 7.3 °C (Fick and Hijmans, 2017). The reconstructed current MAAT [based on the pollen assemblages; $r^2 = 0.77$, RMSEP = 3.6° (Supplementary Table S2)] is 7.7 °C, showing a difference of 0.4 °C. The reconstructed MAAT excluding *Alnus* is 10.5 °C, showing a higher temperature difference of 2.8 °C (Supplementary Fig. S4). Here we show MAAT values (including *Alnus*; Fig. 4). The maximum reconstructed temperature (10.1 °C) was reached at 6.4 cal ka BP, and the minimum (3.9 °C) at 0.9 cal ka BP. The warmest interval (8.7 °C) occurred from 6.5 to 5.5 cal ka BP. After this, a general decreasing trend in temperature occurred over a period of 1500 years, with the coldest period (average = 6.9 °C) between 5.1 and 4.1 cal ka BP. At around 4 cal ka BP a warming is reconstructed, with MAAT reaching mean values of 7.7 °C, characteristic for most of the Late Holocene. Some rapid oscillations interrupting this trend occurred at around 2.8 cal ka BP (6.8 °C), and 0.9 cal ka BP (3.9 °C) (Fig. 4).

4.4. Distribution of brGDGTs

The relative abundances of individual brGDGTs fractions are given in Supplementary Table S3. The brGDGTs distribution in the lake sediment samples is dominated by compounds without cyclopentane rings (Fig. 5A). BrGDGT Ia is the most abundant compound in soil samples, while the hexamethylated brGDGT IIIa is most abundant in lake sediment and SPM samples (Fig. 5). A triplot reveals that lake sediments in general have more of pentamethylated compounds than soil samples (lake >40% vs soil 30–40%) (Fig. 5C). Also, they have in general more (>20%) hexamethylated compounds than soils. Although there are a few (3) soil samples that overlap with the lake sediments in Fig. 5C, both sample types are fairly well separated. The GDGT distribution derived from the SPM sample on the other hand, plots within the range of lake sediment samples (Fig. 5C). The variability in brGDGTs can be summarized further using brGDGT ratios (Fig. 5B and Fig. 5D). The MBT'$_{5ME}$ mean values of lake sediments ($\sim 0.40 \pm 0.04$) is more similar to the MBT'$_{5ME}$ in the SPM (0.42) than to the MBT'$_{5ME}$ in soil that show higher value ($\sim 0.49 \pm 0.07$) (average of the downcore vs soil samples are significantly different, $p < 0.05$) (Fig. 5B). The same occurs for the IR and ΣIIIa/ΣIIa, showing mean values of lake sediments ($0.18 \pm 0.03/0.58 \pm 0.14$, respectively) and soil samples ($0.13 \pm 0.08/0.37 \pm 0.13$, respectively), where the mean values of lake sediments vs soil samples are significantly different ($p < 0.05$) in both ratios. Downcore variations in the MBT'$_{5ME}$ and temperature (based on Martínez-Sosa et al., 2021) have relatively constant values (depicting some shorter oscillations) between 6.5 and 5.4 cal ka BP with mean values of 0.4 (11.3 °C). A decreasing trend occurs from 5.4 cal ka BP to 4.2 cal ka BP, reaching

minimum values (0.36 for MBT'$_{5ME}$; 10.2 °C). After that, an increasing trend starts at 4.2 cal ka BP, interrupted only by two higher values occurring at 3.9 and 3.1 cal ka BP, showing mean values of 0.44 for MBT'$_{5ME}$ (12.1 °C). From 2.2 to 1.3 cal ka BP MBT'$_{5ME}$ mean values reach 0.46 (12.7 °C) (Fig. 6). Downcore, the IR values range between 0.1 and 0.28, showing a decreasing trend with some oscillations from the Middle to Late Holocene (from 6.5 to 0.7 cal ka BP), and an increase from the last 0.7 to 0.2 cal ka BP (Fig. 6). The ΣIIIa/ΣIIa ratio shows an increasing trend from 6.5 to 4.2 cal ka BP with values between 0.87 and 0.30 with a mean value of 0.59, followed by a decrease thorough the Middle to Late Holocene with values ranging from 0. 7 to 0.1 (Fig. 6). The different average IR and ΣIIIa/ΣIIa ratio values of lake sediments and soil samples respectively, will be used to determine a threshold value to identify contributions of watershed soils (IR = 0.13; ΣIIIa/ΣIIa = 0.37; average of soil samples) (Fig. 6).

5. Discussion

5.1. Provenance of the brGDGTs: soils vs lacustrine brGDGTs distribution

In general, our results show a different pattern of brGDGT distributions between the sediment core samples and the soil samples from the Mocearu lake catchment (Fig. 5) with the former samples showing similar values to the SPM sample (Fig. 5), suggesting a dominant in-situ production of brGDGTs.

The Moc-02 record shows an intercalation of different layers between more organic and clastic material (Fig. 3), which can be indicative of a change in the organic matter source. The distribution of brGDGT abundances between organic and clastic facies is similar, i.e., both sediment types have MBT'$_{5ME}$ values that are similar to that obtained from the suspended matter (Fig. 5). However, with MBT'$_{5ME}$ values of 0.39 ± 0.05 for the organic facies and 0.41 ± 0.03 for the clastic ones, small but significant changes in average MBT'$_{5ME}$ values are found between the sediment types (t-test; $p = 0.02$). To constrain the influence of soil-derived brGDGT lipids at specific depths, we will evaluate the brGDGT ratios ΣIIIa/ΣIIa, IR and MBT'$_{5ME}$.

In two previous studies, the ratio ΣIIIa/ΣIIa has been used to determine the provenance of brGDGTs in the marine and freshwater systems (Xiao et al., 2016; Martin et al., 2019). In a marine outflow system, a value below 0.59 indicated a dominant soil source (Xiao et al., 2016). In a French lowland lake (Lake Front), ratio values over 0.8 were attributed to a dominant aquatic source (Martin et al., 2019). At our site, catchment soils are characterized by a wide range in ΣIIIa/ΣIIa values (0.2–0.73, average = 0.38), whereas downcore samples (range: 0.30 to 0.87) show increased average values of 0.58. The significantly different means (t-test, $p < 0.01$) support a dominant aquatic source of the sedimentary brGDGTs (Figs. 5, 6). However, the range in ΣIIIa/ΣIIa values downcore suggests a possible minor contribution of soil material that can be variable through time. To identify those depths with a soil contribution, ratios that show significantly different values, and thus allow to distinguish, between downcore (lacustrine) and soil distributions respectively (ΣIIIa/ΣIIa decrease, IR decrease, MBT'$_{5ME}$ increase) are compared. Evaluated together with lithological changes and pollen signature they can indicate catchment erosion (Fig. 6; Supplementary Fig. S1). The threshold value of the ΣIIIa/ΣIIa and IR ratio that is indicative of a soil signature is determined at 0.37 and 0.13, respectively (Fig. 6, average of soil ΣIIIa/ΣIIa and IR ratio values). During the periods 3.9 to 3.3 cal ka BP and 2.2 to 0.9 cal ka BP, all ratio values indicate an increased soil input. This suggests increased soil erosion on the catchment and will be taken into account when discussing the paleotemperature reconstructions (Fig. 7).

5.2. Pollen and brGDGT temperature reconstructions

5.2.1. Offset between pollen and brGDTG temperature reconstructions

The temperature reconstruction from brGDGTs is based on the global

lake calibration from Raberg et al. (2021) and the global Bayesian lacustrine calibration from Martínez-Sosa et al. (2021). Both studies consider that brGDGT-inferred temperature values for locations with high seasonality where the lake is ice-covered a part of the year are expected to reflect their preferred growing conditions. As such, they calibrate the MBT'$_{5ME}$ in their global datasets against MAF. As Lake Mocearu is a high seasonality lake, the ice and snow cover during winter can be a reason for a seasonal bias in the brGDGT production, and we therefore adopt a MAF reconstruction based on these organic biogeochemical proxies. The actual temperature of the warmest quarter at Mocearu Lake area is 16.6 °C (WorldClim; Fick and Hijmans, 2017). The MAF temperature reconstructed based on brGDGT (mean temperature 14 °C) indeed falls between this value and the actual mean temperature (7.3 °C). In addition to this, the MAAT reconstruction based on pollen shows values that are similar to the actual mean temperature in the Lake Mocearu area (Fig. 4). The MAAT (based on pollen) and MAF (based on brGDGT) reconstructions show similar trends during the Middle Holocene ($r^2 = 0.56$ for from 6.5 to 4.2 cal ka BP), with a mean temperature anomaly (ΔT) between them of 3.6 °C (Fig. 7). However, higher discrepancies between the two temperature curves appear during the Late Holocene showing a ΔT mean values of 5.1 °C (Fig. 7). The MAAT temperature decreases from the Middle to Late Holocene, as in many other Europeans records (Fig. 8, c-d). However, the reconstructed MAF shows unexpectedly high mean values during the Late Holocene when compared with other Europeans records (Fig. 8, c-d). The increase in MAF during the Late Holocene could be due to two reasons. Firstly, it is possible that a higher terrestrial organic matter input to the lake during the Late Holocene mainly occurred around 3.9 to 3.3 cal ka BP and from 2.2 to 0.9 cal ka BP (Figs. 6, 7 and 8), influenced the sedimentary MBT'$_{5ME}$ values, resulting in increased values. The high values occur at the horizons where we reconstructed increased soil input (Fig. 6). Indeed, at the location under study, the temperature can be overestimated with as much as 2.3 °C when the lacustrine calibration is applied to catchment soils (Supplementary Fig. S6). Secondly, there may have been a change in the lake system to a lower water table, indicated

by a higher occurrence of wetland plants after 4.2 ka BP (see Cyperaceae pollen curve in Supplementary Fig.S1), the increase in organic matter (higher LOI$_{550}$; Fig. 6), and the decrease in IR and CBT' through time (Fig. 6). These changes in IR and CBT' (after 4.2 cal ka BP; Fig. 6) can be indicative of a change in the brGDGTs producers' community in soils, although the impact on MBT'$_{5ME}$ values is still poorly confined in lacustrine environments (De Jonge et al., 2021).

5.2.2. Disentangling MAAT and MAF temperature offset during the Late Holocene

A decreasing trend in MAAT temperature during the Late Holocene is reconstructed, while higher temperatures are recorded in MAF, intensified from 3.9 to 3.4 cal ka BP and from 2.2 to 0.9 cal ka BP. These differences between MAAT and MAF during the Late Holocene have been discussed above (section 5.2.1), possibly related to increased soil input to the lake, and/or a change in lake chemistry, after 4.2 cal ka BP (Fig. 6). The increase in soil input could be due to natural or anthropogenic causes. Moderate anthropogenic influences can be derived from the pollen record. Although four pollen grains from cultivate plants such as Cerealia-type were only found in the last 0.4–0.2 cal ka BP, a slight increase in other human indicator pollen types, such as *Plantago lanceolata* and *P. major* type, occurs after 4.2 cal ka BP. This increase in human indicator pollen types starting during the Bronze Age has also been detected in other records in east-central Europe (Vincze et al., 2019). A decrease in lake level and/or high seasonal fluctuations in the water table since the 5.4–4.2 climatic transition, is suggested to be related to the increase in emergent wetland plant communities in the lake shore (Fig. 6; Supplementary Fig. S1). This also corresponds with the expansion of *Fagus* pollen after 4.2 cal yr BP, this could be indicative of decrease water level and/or colder temperatures (Magyari et al., 2009). This agrees with the proposed change in the lake chemistry after 4.2 cal ka BP. However, superimposed on this long-term lower water table period, a climatic driver of the changed provenance of brGDGTs between 3.9 and 3.4 cal yr BP (coinciding with Bond event 3) and 2.2 to 0.9 cal ka BP (coinciding with Bond event 1) (Fig. 7) can be related to the
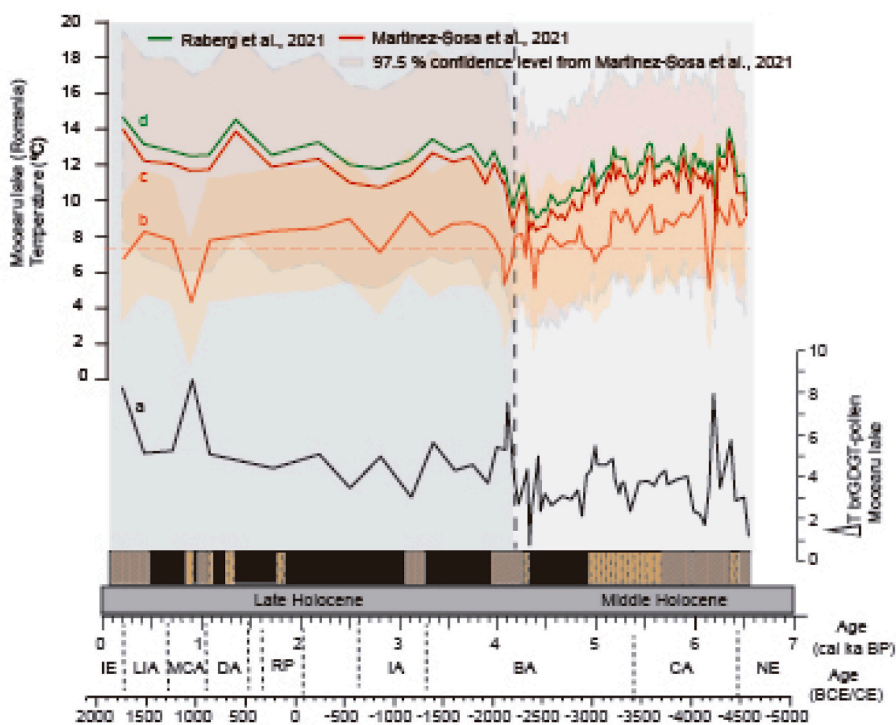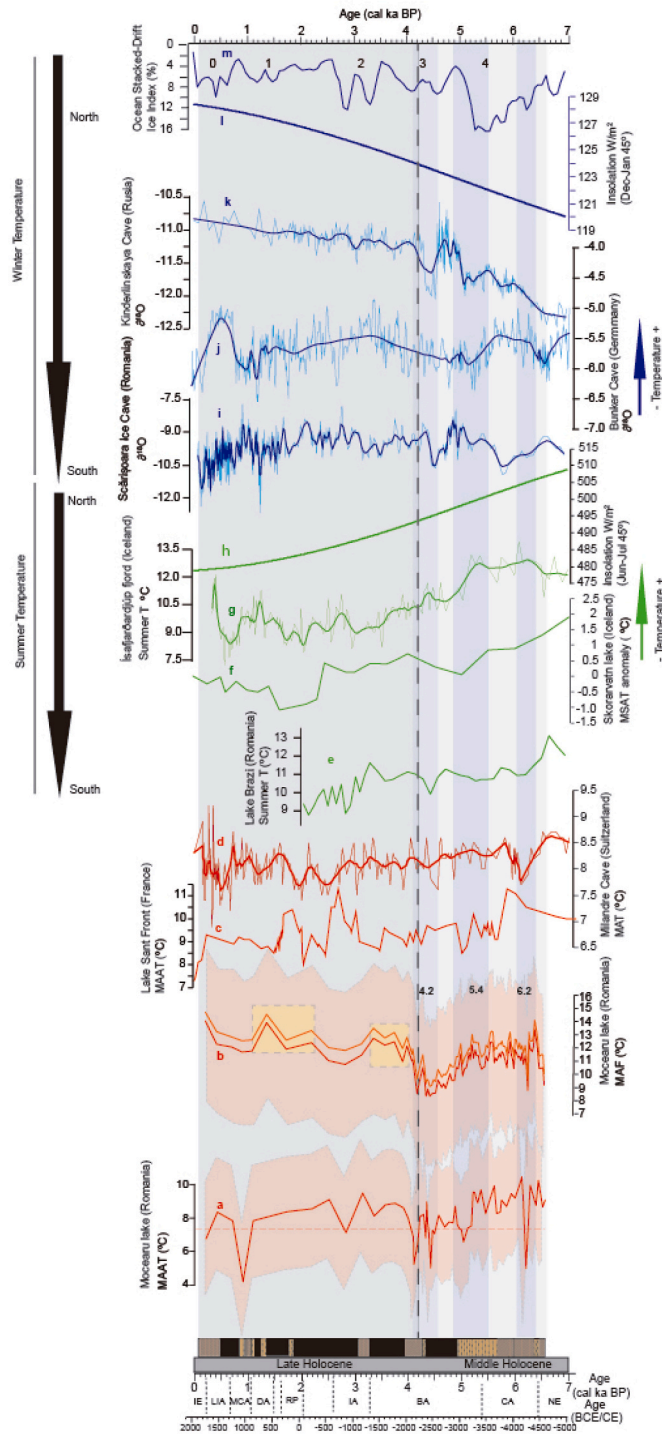

Fig. 7. Comparison between temperature reconstruction based on pollen, mean annual air temperature (MAAT) and brGDGT, mean temperature of months above freezing (MAF). a) Temperature anomaly between brGDGT and pollen temperature reconstructions from the Moc-02 record, b) MAAT reconstructed, orange shadow displays the standard error of the reconstruction c) MAF reconstructed.

Fig. 8. Comparison of different mean summer, winter, and annual temperature reconstructions in northern Europe during the last 6.5 cal ka BP. a) MAAT reconstruction based on pollen from the Moc-02 record (this study), b) MAF reconstruction based on brGDGT from Moc-02 record (this study) with Raberg et al. (2021) (orange line) and Martínez-Sosa et al. (2021) calibration sets (red line), c) MAAT reconstruction based on brGDGT data from Lake Sant Front (Martin et al., 2020), d) MAT reconstruction from Milandre Cave (Affolter et al., 2019), e) Summer temperature reconstruction from Lake Brazi (Tóth et al., 2015), f) Mean summer air temperature (MSTA) anomaly based on brGDGT data from Skorarvatn lake in Iceland (Harning et al., 2020), g) Summer temperature reconstruction from Ísafjarðardjúp fjord (Moossen et al., 2015), h) Summer insolation calculated for 45°N (Laskar et al., 2004), i) $\partial^{18}O$ reconstruction from Scărişoara Ice Cave (Perşoiu et al., 2017), j) $\partial^{18}O$ reconstruction from Bunker Cave (Fohlmeister et al., 2012), k) $\partial^{18}O$ reconstruction from Kinderlinskaya Cave (Baker et al., 2017), l) Winter insolation calculated for 45°N (Laskar et al., 2004), m) Ocean stacked percentage of the Drift Ice Index (reversed) from the North Atlantic (Bond et al., 2001). Vertical blue shadows are related with cold events. Vertical dashline is the division line between the Middle-Late Holocene. Yellow shadows in (c) are related with soil input periods. Acronyms: IE = Industrial Era, LIA = Little Ice Age, MCA = Medieval Climate Anomaly, RP = Roman Period, IA = Iron Age, BA = Bronze Age, CA = Chalcolithic, NE = Neolithic. (For interpretation of the references to colour in this figure legend, the reader is referred to the web version of this article.)

increase in precipitation (Supplementary Fig. S5) (and higher terrestrial input to the lake). This enhanced rainfall is reported for these periods in the Southern Carpathians (Longman et al., 2017a, 2019). Most paleoclimate archives from this region suggest that from 3.1–2.8 cal ka BP available moisture and annual precipitation increased strongly resulting in maximum Holocene water levels in lakes and high mire surface wetness values on peat bogs in the Eastern Carpathians (Schnitchen et al., 2006; Magyari et al., 2009; Jakab and Sümegi, 2010; Longman et al., 2017b; Buczkó et al., 2019).

5.3. Paleoclimate variability

5.3.1. Middle to Late Holocene climate transition

Many studies suggest that the Holocene Thermal Maximum (HTM) occurred in the northern hemisphere during the Early and Middle Holocene, with a subsequent gradual temperature decrease that started around 6 cal ka BP and continued into the Late Holocene (Renssen et al., 2009; Wanner et al., 2015; Moossen et al., 2015; Haliuc et al., 2017). Our proxy record, that covers this Middle to Late Holocene transition, is marked by an abrupt temperature drop between 5.4 and 4.2 cal ka BP. This temperature drop is identified in both MAAT and MAF reconstructions. Prior to this transition, mean MAAT and MAF temperature values are higher from 6.5 to 5.4 cal ka BP, similar with other MAAT reconstruction from central Europe (Martin et al., 2020; Affolter et al., 2019; Fig. 7). This warmer period agrees with the HTM period correlated with summer temperature reconstruction from eastern (Tóth et al., 2015; Fig. 7) and northern (Moossen et al., 2015; Harning et al., 2020 Fig. 7) European records. These warmer conditions during the Middle Holocene are compatible with a higher summer insolation (Fig. 7). On the contrary, winter temperature reconstructions from eastern Europe (Perşoiu et al., 2017) and northern latitudes (Fohlmeister et al., 2012; Baker et al., 2017) show lower temperature values in correlation with a lower winter insolation during the Middle Holocene (Fig. 7). This gradual summer insolation decrease and winter insolation increase result in a lower seasonality from the end of the Middle Holocene to the Late Holocene (Perşoiu et al., 2017). At Mocerau Lake the Middle to Late Holocene transition is characterized by a decrease in temperature after around 5.4–4.2 cal ka BP. Cooling in the pollen-inferred MAAT values is driven by the decrease in some thermophilus taxa (*Corylus*, *Ulmus*, *Tilia*) and the *Alnus* expansion. As in the modern day pollen rain of Europe *A. glutinosa* is more abundant in cool temperate sites in Northern and North-Central Europe and the British Isles (Brewer et al., 2017). In addition to temperature, its presence also reflects a change in

precipitation. Since this species is well-adapted to growing on very wet soils, its expansion at different times at different sites suggests local differences in soil moisture conditions (Houston Durrant et al., 2016). Looking at other pollen records in this region (Bisoca, 890 m a.s.l. Tantau et al., 2003) and the autoecology of *A. glutinosa* (Houston Durrant et al., 2016), they suggest that regionally this period coincides with maximum share of *Carpinus betulus* in the mid altitude forests, and *A. glutinosa* expansion can likely be explained by temperature and humidity trends between 5.6 and 3.5 cal ka BP (Tantau et al., 2003; Magyari et al., 2009). At Mocearu it likely expanded on the seasonally wet lakeshore and its expansion was likely facilitated by lake level decrease and/or high seasonal fluctuation in lake level. The vegetation changes thus support general cooling in summer temperatures, and also hints at a regime shift in precipitation pattern that resulted in the development of seasonally exposed lakeshores at Mocearu.

We hypothesize that this temperature decrease occurring during the Middle to Late Holocene transition is related to a shift from consistent NAO- conditions to a predominance of NAO+ phase until present, agreeing with the actual climate system over the western Romania where Mediterranean cyclones are activated mostly during autumn and early winter (Georgescu and Stefan, 2010; Magyari et al., 2013; Perşoiu et al., 2017). This shift in climate conditions since the Middle- to Late Holocene transition has been identified in other Mediterranean and North Atlantic areas (Debret et al., 2009; Fletcher et al., 2013; Ramos-Román et al., 2018).

5.3.2. Rapid climatic changes during the Middle Holocene

The higher resolution section of the Moc-02 record between 6.5 and 4.2 cal yr BP allows us to describe rapid climatic changes during the Middle to Late Holocene transition, based on MAAT and MAF reconstructions. Through a spectral analysis (Supplementary Fig. S7), we can identify a cyclicity of around 330–370 yrs. This periodicity is marked by temperature decreases occurring at 6.2, 5.4, 5.0, 4.7 and 4.2 cal yr BP, these events have been identified in both temperature reconstructions. The most pronounced events occur at 6.2, 5.0 and 4.2 cal ka BP, with MAAT decrease with respect to the mean during the Middle Holocene (8.3 °C) of 3.3, 1.7 and 3. 3 °C, respectively (Fig. 7). These climatic events have been described in the Carpathian region (Schöll-Barna et al., 2012; Demény et al., 2013, 2021; Magyari et al., 2009; Magyari et al., 2013; Drăguşin et al., 2014; Diaconu et al., 2017; Longman et al., 2017a; Haliuc et al., 2017; Túri et al., 2021), and in the western Mediterranean as cold events (Zielhofer et al., 2017; Ramos-Román et al., 2018). These short climatic events during the Middle Holocene, have also been recorded as short-lived declines in biomass (with a fire frequency of 317 yr) in the Carpathians and are associated with cooling events (Feurdean et al., 2013). Two of the most significant climatic events during the Middle Holocene detected in the Northern Hemisphere are the one around 5.4 cal ka BP (Orme et al., 2021; Sicre et al., 2021) and the worldwide 4.2 cal ka BP climatic event (Bar-Matthews et al., 1998; Bond et al., 2001; Mayewski et al., 2004; Liu and Feng, 2012; Ran and Chen, 2019). Recently, the event dated around 5.4 cal ka BP has been recorded in some North Atlantic records as one of the coldest periods during the Middle Holocene (Orme et al., 2021; Sicre et al., 2021), coinciding with the major drift ice described by Bond et al. (2001), Bond event 4 (Fig. 7), and the beginning of the Neoglacial cooling in the northern latitudes (Renssen et al., 2009). This cold period has been related to the decline of the northern hemisphere summer insolation, the decay of the Subpolar Gyre, the Atlantic Meridional Overturning Circulation, and the High Iceland-Scotland Overflow Water (Sicre et al., 2021). These events have been also detected in East-Central Europe. The impact of the 5.4 cal ka BP event had been assessed in eastern Europe as a strong desiccation in the Lake Balaton (Pálfi et al., 2021). The 4.2 cal ka BP event has been detected in the Carpathians area showing a decrease in temperature (Constantin et al., 2007; Feurdean et al., 2008; Tóth et al., 2015; Perşoiu et al., 2017; Fig. 6), and a significant forest decline suggesting drier conditions (Feurdean et al., 2015;

Vincze et al., 2017; Orbán et al., 2018). In the study of Feurdean et al. (2015) two drops in temperature occurring at around 5 and 4.2 cal ka BP are superimposed on a cold trend that starts at 5.4 cal ka BP.

6. Conclusions

The study of the Mocearu record in the Eastern Carpathians has provided information about the mean annual air temperature (MAAT) and mean temperature above freezing (MAF) during the Middle and Late Holocene. The MAAT and MAF have provided new paleoclimate data for this region, reporting a temperature decrease from the Middle to the Late Holocene that agree with other Northern Hemisphere records. The multiproxy approach allows a reliable temperature reconstruction, when brGDGT (MAF) and pollen (MAAT) temperature reconstructions covary, i.e. between 6.5 and 4.2 cal ka BP. The temperature trend during the Middle Holocene is superimposed by several abrupt declines occurring in both MAF and MAAT reconstructions at 6.2, 5.4 and 4.2 cal ka BP, featuring a prominent decrease from 5.4 to 4.2 cal ka BP (from 12 to 9 °C MAF) coinciding with the beginning of the Neoglacial cooling in northern latitudes. After 4.2 cal ka BP, a discrepancy between MAAT and MAF occurs, MAAT show a decrease associated with other Northern Hemisphere records while MAF increase. Here, a change in the lake record is detected by lower values of the IR, and ΣIIIa/ΣIIa, that can be linked with an increased in soil input to the lake and/or a change in the brGDGT community. This is coeval with the occurrence of plants related with human land use and the increase in emergent wetland plants. The multiproxy approach at Mocearu Lake thus results in a high-resolution (65 yr) view on the Middle to Late Holocene transition temperature change, revealing both high cyclicity (330–370 yr) as a long-term well-expressed temperature decrease, culmination in a well-expressed 4.2 ka cold event at this location. Further research will expand on this by linking archaeological evidence of human migrations in this time window, and by exploring the changes in atmospheric circulation that can cause this well-expressed climate transition.

Declaration of Competing Interest

The authors declare that they have no known competing financial interests or personal relationships that could have appeared to influence the work reported in this paper.

Appendix A. Supplementary data

Supplementary data to this article can be found online at https://doi.org/10.1016/j.gloplacha.2022.103859.

References

Affolter, S., Häuselmann, A., Fleitmann, D., Edwards, R.L., Cheng, H., Leuenberger, M., 2019. Central Europe temperature constrained by speleothem fluid inclusion water

isotopes over the past 14,000 years. Sci. Adv. 5 (6), eaav3809. https://doi.org/10.1126/sciadv.aav3809.

Bahr, A., Jiménez-Espejo, F.J., Kolasinac, N., Grunert, P., Hernández-Molina, F.J., Röhl, U., Voelker, A.H., Escutia, C., Stow, D.A., Hodell, D., 2014. Deciphering bottom current velocity and paleoclimate signals from contourite deposits in the G ulf of C ádiz during the last 140 kyr: an inorganic geochemical approach. Geochem. Geophys. Geosyst. 15 (8), 3145–3160.

Baker, J.L., Lachniet, M.S., Chervyatsova, O., Asmerom, Y., Polyak, V.J., 2017. Holocene warming in western continental Eurasia driven by glacial retreat and greenhouse forcing. Nat. Geosci. 10 (6), 430–435. https://doi.org/10.1038/ngeo2953.

Bar-Matthews, M., Ayalon, A., Kaufman, A., 1998. Middle to Late Holocene (6,500 Yr. Period) Paleoclimate in the Eastern Mediterranean Region from Stable Isotopic Composition of Speleothems from Soreq Cave, Israel. In: Issar, A.S., Brown, N. (Eds.), Water, Environment and Society in Times of Climatic Change: Contributions from an International Workshop within the framework of International Hydrological Program (IHP) UNESCO, held at Ben-Gurion University, Sede Boker, Israel from 7–12 July 1996. Springer Netherlands, pp. 203–214. https://doi.org/10.1007/978-94-017-3659-6_9.

Bartholy, J., Pongrácz, R., Gelybó, G., 2009. Climate signals of the North Atlantic Oscillation detected in the Carpathian basin. Appl. Ecol. Environ. Res. 7 (3), 229–240.

Beug, H.-J., 2004. Leitfaden der Pollenbestimmung für Mitteleuropa und angrenzende Gebiete. Fischer, Stuttgart, p. 61.

Biagioni, F., Rapetti, F., 2005. Climatic features of the Muscel Valley (Buzău Subcarpathians, Romania) as from the registered data during 1961-2003. Revista de Geomorfologie 7, 107–119.

Bini, M., Zanchetta, G., Perşoiu, A., Cartier, R., Català, A., Cacho, I., Dean, J.R., Di Rita, F., Drysdale, R.N., Finnè, M., Isola, I., Jalali, B., Lirer, F., Magri, D., Masi, A., Marks, L., Mercuri, A.M., Peyron, O., Sadori, L., Brisset, E., 2019. The 4.2 ka BP Event in the Mediterranean region: an overview. Clim. Past 15 (2), 555–577. https://doi.org/10.5194/cp-15-555-2019.

Birks, H., Braak, C.T., Line, J., Juggins, S., Stevenson, A., 1990. Diatoms and pH reconstruction. Philos. Trans. Roy. Soc. London. B, Biological Sciences 327 (1240), 263–278.

Blaauw, M., Christen, J.A., 2011. Flexible paleoclimate age-depth models using an autoregressive gamma process. Bayesian Anal. 6 (3), 457–474.

Bojariu, R., Paliu, D.-M., 2001. North Atlantic Oscillation Projection on Romanian climate Fluctuations in the Cold season. In: India, M.B., Bonillo, D.L. (Eds.), Detecting and Modelling Regional Climate Change. Springer, Berlin Heidelberg, pp. 345–356. https://doi.org/10.1007/978-3-662-04313-4_29.

Bond, G., Kromer, B., Beer, J., Muscheler, R., Evans, M.N., Showers, W., Hoffmann, S., Lotti-Bond, R., Hajdas, I., Bonani, G., 2001. Persistent solar influence on North Atlantic climate during the holocene. Science 294 (5549), 2130. https://doi.org/10.1126/science.1065680.

Brewer, S., Giesecke, T., Davis, B.A., Finsinger, W., Wolters, S., Binney, H., de Beaulieu, J.-L., Fyfe, R., Gil-Romera, G., Kühl, N., 2017. Late-glacial and Holocene European pollen data. J. Maps 13 (2), 921–928.

Buczkó, K., Ács, É., Báldi, K., Pozderka, V., Braun, M., Kiss, K.T., Korponai, J., 2019. The first high resolution diatom record from Lake Balaton, Hungary in Central Europe. Limnetica 38 (1), 417–430.

Chevalier, M., Davis, B.A., Heiri, O., Seppä, H., Chase, B.M., Gajewski, K., Lacourse, T., Telford, R.J., Finsinger, W., Guiot, J., 2020. Pollen-based climate reconstruction techniques for late Quaternary studies. Earth Sci. Rev. 103384.

Constantin, S., Bojar, A.-V., Lauritzen, S.-E., Lundberg, J., 2007. Holocene and Late Pleistocene climate in the sub-Mediterranean continental environment: a speleothem record from Poleva Cave (Southern Carpathians, Romania). Palaeogeogr. Palaeoclimatol. Palaeoecol. 243 (3), 322–338. https://doi.org/10.1016/j.palaeo.2006.08.001.

Core, R., 2015. Team. R: A Language and Environment for Statistical Computing, 3, p. 2.

Davis, B.A.S., Brewer, S., Stevenson, A.C., Guiot, J., 2003. The temperature of Europe during the Holocene reconstructed from pollen data. Quat. Sci. Rev. 22 (15), 1701–1716. https://doi.org/10.1016/S0277-3791(03)00173-2.

Davis, B.A.S., Chevalier, M., Sommer, P., Carter, V.A., Finsinger, W., Mauri, A., Phelps, L. N., Zanon, M., Abegglen, R., AAkesson, C.M., Alba-Sánchez, F., Anderson, R.S., Antipina, T.G., Atanassova, J.R., Beer, R., Belyanina, N.I., Blyakharchuk, T.A., Borisova, O.K., Bozilova, E., Zimny, M., 2020. The Eurasian Modern Pollen Database (EMPD), Version 2. Earth Syst. Sci. Data Discuss. 2020, 1–41. https://doi.org/10.5194/essd-2020-14.

De Jonge, C., Hopmans, E.C., Stadnitskaia, A., Rijpstra, W.I.C., Hofland, R., Tegelaar, E., Sinninghe Damsté, J.S., 2013. Identification of novel penta- and hexamethylated branched glycerol dialkyl glycerol tetraethers in peat using HPLC–MS2, GC–MS and GC–SMB-MS. Org. Geochem. 54, 78–82. https://doi.org/10.1016/j.orggeochem.2012.10.004.

De Jonge, C., Radujković, D., Sigurdsson, B.D., Weedon, J.T., Janssens, I., Peterse, F., 2019. Lipid biomarker temperature proxy responds to abrupt shift in the bacterial community composition in geothermally heated soils. Org. Geochem. 137 https://doi.org/10.1016/j.orggeochem.2019.07.006.

De Jonge, C., Stadnitskaia, A., Hopmans, E.C., Cherkashov, G., Fedotov, A., Streletskaya, I.D., Vasiliev, A.A., Damsté, J.S.S., 2015. Drastic changes in the distribution of branched tetraether lipids in suspended matter and sediments from the Yenisei River and Kara Sea (Siberia): implications for the use of brGDGT-based proxies in coastal marine sediments. Geochim. Cosmochim. Acta 165, 200–225.

De Jonge, C., Hopmans, E.C., Zell, C.I., Kim, J.-H., Schouten, S., Sinninghe Damsté, J.S., 2014. Occurrence and abundance of 6-methyl branched glycerol dialkyl glycerol tetraethers in soils: Implications for palaeoclimate reconstruction. Geochim. Cosmochim. Acta 141, 97–112.

De Jonge, C., Kuramae, E.E., Radujković, D., Weedon, J.T., Janssens, I.A., Peterse, F., 2021. The influence of soil chemistry on branched tetraether lipids in mid-and high latitude soils: implications for brGDGT-based paleothermometry. Geochim. Cosmochim. Acta 310, 95–112.

Dean, W.E., 1974. Determination of carbonate and organic matter in calcareous sediments and sedimentary rocks by loss on ignition: comparison with other methods. J. Sediment. Petrol. 44.

Debret, M., Sebag, D., Crosta, X., Massei, N., Petit, J.-R., Chapron, E., Bout-Roumazeilles, V., 2009. Evidence from wavelet analysis for a mid-Holocene transition in global climate forcing. Quat. Sci. Rev. 28 (25–26), 2675–2688. https://doi.org/10.1016/j.quascirev.2009.06.005.

Demény, A., Czuppon, G., Siklósy, Z., Leél-Őssy, S., Lin, K., Shen, C.-C., Gulyás, K., 2013. Mid-Holocene climate conditions and moisture source variations based on stable H, C and O isotope compositions of speleothems in Hungary. Quat. Int. 293, 150–156.

Demény, A., Kern, Z., Hatvani, I.G., Torma, C., Topál, D., Frisia, S., Leél-Őssy, S., Czuppon, G., Surányi, G., 2021. Holocene hydrological changes in Europe and the role of the North Atlantic ocean circulation from a speleothem perspective. Quat. Int. 571, 1–10.

Diaconu, A.-C., Toth, M., Lamentowicz, M., Heiri, O., Kuske, E., Tanțău, I., Panait, A.-M., Braun, M., Feurdean, A., 2017. How warm? How wet? Hydroclimate reconstruction of the past 7500 years in northern Carpathians, Romania. Palaeogeogr. Palaeoclimatol. Palaeoecol. 482, 1–12.

Drăguşin, V., Staubwasser, M., Hoffmann, D.L., Ersek, V., Onac, B.P., Veres, D., 2014. Constraining Holocene hydrological changes in the Carpathian–Balkan region using speleothem δ^{18}O and pollen-based temperature reconstructions. Clim. Past 10 (4), 1363–1380. https://doi.org/10.5194/cp-10-1363-2014.

Faegri, K., Iversen, J., 1989. Textbook of Pollen Analysis. Wiley, New York.

Fărcaş, I., Sorocovschi, V., 1992. The climate of the Retezat mountains. In: Parcul Național Retezat. Studii Ecologice. POPOVICI I. Edit. West Side Computers Brașov, pp. 13–20.

Feurdean, A., Klotz, S., Mosbrugger, V., Wohlfarth, B., 2008. Pollen-based quantitative reconstructions of Holocene climate variability in NW Romania. Palaeogeogr. Palaeoclimatol. Palaeoecol. 260 (3), 494–504. https://doi.org/10.1016/j.palaeo.2007.12.014.

Feurdean, A., Liakka, J., Vannière, B., Marinova, E., Hutchinson, S.M., Mosburger, V., Hickler, T., 2013. 12,000-years of fire regime drivers in the lowlands of Transylvania (Central-Eastern Europe): a data-model approach. Quat. Sci. Rev. 81, 48–61. https://doi.org/10.1016/j.quascirev.2013.09.014.

Feurdean, A., Marinova, E., Nielsen, A.B., Liakka, J., Veres, D., Hutchinson, S.M., Braun, M., Timar-Gabor, A., Astalos, C., Mosburgger, V., Hickler, T., 2015. Origin of the forest steppe and exceptional grassland diversity in Transylvania (central-eastern Europe). J. Biogeogr. 42 (5), 951–963. https://doi.org/10.1111/jbi.12468.

Fick, S.E., Hijmans, R.J., 2017. WorldClim 2: New 1-km spatial resolution climate surfaces for global land areas. Int. J. Climatol. 37 (12), 4302–4315.

Fletcher, W.J., Debret, M., Goñi, M.F.S., 2013. Mid-Holocene emergence of a low-frequency millennial oscillation in western Mediterranean climate: implications for past dynamics of the North Atlantic atmospheric westerlies. The Holocene 23 (2), 153–166. https://doi.org/10.1177/0959683612460783.

Fohlmeister, J., Vollweiler, N., Spötl, C., Mangini, A., 2012. COMNISPA II: update of a mid-European isotope climate record, 11 ka to present. The Holocene 23 (5), 749–754. https://doi.org/10.1177/0959683612465446.

Georgescu, F., Stefan, S., 2010. Cyclonic activity over Romania in connection with the air circulation types. Rom. Rep. Phys 62 (4), 878–886.

Haliuc, A., Veres, D., Brauer, A., Hubay, K., Hutchinson, S.M., Begy, R., Braun, M., 2017. Palaeohydrological changes during the mid and late Holocene in the Carpathian area, Central-Eastern Europe. Glob. Planet. Chang. 152, 99–114. https://doi.org/10.1016/j.gloplacha.2017.02.010.

Harning, D.J., Curtin, L., Geirsdóttir, Á., D'Andrea, W.J., Miller, G.H., Sepúlveda, J., 2020. Lipid biomarkers quantify Holocene summer temperature and ice cap sensitivity in Icelandic lakes. Geophys. Res. Lett. 47 (3) https://doi.org/10.1029/2019GL085728 e2019GL085728.

Heiri, O., Lotter, A.F., Lemcke, G., 2001. Loss on ignition as a method for estimating organic and carbonate content in sediments: Reproducibility and comparability of results. J. Paleolimnol. 25 (1), 101–110. https://doi.org/10.1023/A:1008119611481.

Hopmans, E.C., Schouten, S., Sinninghe Damsté, J.S., 2016. The effect of improved chromatography on GDGT-based palaeoproxies. Org. Geochem. 93, 1–6. https://doi.org/10.1016/j.orggeochem.2015.12.006.

Houston Durrant, T., de Rigo, D., Caudullo, G., 2016. Alnus glutinosa in Europe: distribution, habitat, usage and threats. European Atlas of Forest Tree Species 64–65.

Huguet, C., Hopmans, E.C., Febo-Ayala, W., Thompson, D.H., Sinninghe Damsté, J.S., Schouten, S., 2006. An improved method to determine the absolute abundance of glycerol dibiphytanyl glycerol tetraether lipids. Org. Geochem. 37, 1036–1041.

Jakab, G., Sümegi, P., 2010. Preliminary data on the bog surface wetness from the Sirok Nyírjes-tó peat bog, Mátra Mts, Hungary. Central Eur. Geol. 53 (1), 43–65.

Juggins, S., 2009. Rioja: An R Package for the Analysis of Quaternary Science Data. New Castle, UK.

Juggins, S., Birks, H.J.B., 2012. Quantitative environmental reconstructions from biological data. In: Tracking Environmental Change Using Lake Sediments. Springer, pp. 431–494.

Kaufman, D.S., Ager, T.A., Anderson, N.J., Anderson, P.M., Andrews, J.T., Bartlein, P.J., Brubaker, L.B., Coats, L.L., Cwynar, L.C., Duvall, M.L., Dyke, A.S., Edwards, M.E., Eisner, W.R., Gajewski, K., Geirsdóttir, A., Hu, F.S., Jennings, A.E., Kaplan, M.R., Kerwin, M.W., Wolfe, B.B., 2004. Holocene thermal maximum in the western Arctic (0–180°W). Quat. Sci. Rev. 23 (5), 529–560. https://doi.org/10.1016/j.quascirev.2003.09.007.

Kern, Z., Balogh, D., Nagy, B., 2004. Investigations for the actual elevation of the mountain permafrost zone on postglacial landforms in the head of Lăpuşnicu Mare Valley, and the history of deglaciation of Ana Lake—Judele Peak region, Retezat Mountains, Romania. Analele Universităţii de Vest Din Timişoara, Geografie 14, 119–132.

Kylander, M.E., Ampel, L., Wohlfarth, B., Veres, D., 2011. High-resolution X-ray fluorescence core scanning analysis of Les Echets (France) sedimentary sequence: new insights from chemical proxies. J. Quat. Sci. 26, 109–117. https://doi.org/10.1002/jqs.1438.

Laskar, J., Robutel, P., Joutel, F., Gastineau, M., Correia, A.C.M., Levrard, B., 2004. A long-term numerical solution for the insolation quantities of the Earth. A&A 428 (1), 261–285. https://doi.org/10.1051/0004-6361:20041335.

Liu, F., Feng, Z., 2012. A dramatic climatic transition at ~4000 cal. Yr BP and its cultural responses in Chinese cultural domains. The Holocene 22 (10), 1181–1197. https://doi.org/10.1177/0959683612441839.

Longman, J., Ersek, V., Veres, D., Salzmann, U., 2017a. Detrital events and hydroclimate variability in the Romanian Carpathians during the mid-to-late Holocene. Quat. Sci. Rev. 167, 78–95. https://doi.org/10.1016/j.quascirev.2017.04.029.

Longman, J., Veres, D., Ersek, V., Haliuc, A., Wennrich, V., 2019. Runoff events and related rainfall variability in the Southern Carpathians during the last 2000 years. Sci. Rep. 9, 5334. https://doi.org/10.1038/s41598-019-41855-1.

Longman, J., Veres, D., Ersek, V., Salzmann, U., Hubay, K., Bormann, M., Wennrich, V., Schäbitz, F., 2017b. Periodic input of dust over the Eastern Carpathians during the Holocene linked with Saharan desertification and human impact. Clim. Past 13 (7), 897–917. https://doi.org/10.5194/cp-13-897-2017.

Magyari, E., Buczkó, K., Jakab, G., Braun, M., Pál, Z., Karátson, D., Pap, I., 2009. Palaeolimnology of the last crater lake in the Eastern Carpathian Mountains: a multiproxy study of Holocene hydrological changes. Hydrobiologia 631 (1), 29–63.

Magyari, E.K., Demény, A., Buczkó, K., Kern, Z., Vennemann, T., Fóriz, I., Vincze, I., Braun, M., Kovács, J.I., Udvardi, B., Veres, D., 2013. A 13,600-year diatom oxygen isotope record from the South Carpathians (Romania): Reflection of winter conditions and possible links with North Atlantic circulation changes. Quat. Int. 293, 136–149. https://doi.org/10.1016/j.quaint.2012.05.042.

Magyari, E., Vincze, I., Orbán, I., Bíró, T., Pál, I., 2018. Timing of major forest compositional changes and tree expansions in the Retezat Mts during the last 16,000 years. Providing Long Environmental Records of Late Quaternary Climatic Oscillations in the South Carpathian Retezat Mountains (PROLONG 477, 40–58. https://doi.org/10.1016/j.quaint.2017.12.054.

Martin, C., Ménot, G., Thouveny, N., Davtian, N., Andrieu-Ponel, V., Reille, M., Bard, E., 2019. Impact of human activities and vegetation changes on the tetraether sources in Lake St Front (Massif Central, France). Org. Geochem. 135, 38–52. https://doi.org/10.1016/j.orggeochem.2019.06.005.

Martin, C., Ménot, G., Thouveny, N., Peyron, O., Andrieu-Ponel, V., Montade, V., Davtian, N., Reille, M., Bard, E., 2020. Early Holocene thermal maximum recorded by branched tetraethers and pollen in Western Europe (Massif Central, France). Quat. Sci. Rev. 228, 106109 https://doi.org/10.1016/j.quascirev.2019.106109.

Martínez-Sosa, P., Tierney, J.E., Stefanescu, I.C., Dearing Crampton-Flood, E., Shuman, B.N., Routson, C., 2021. A global Bayesian temperature calibration for lacustrine brGDGTs. Geochim. Cosmochim. Acta 305, 87–105. https://doi.org/10.1016/j.gca.2021.04.038.

Mayewski, P.A., Rohling, E.E., Stager, J.C., Karlén, W., Maasch, K.A., Meeker, L.D., Meyerson, E.A., Gasse, F., van Kreveld, S., Holmgren, K., Lee-Thorp, J., Rosqvist, G., Rack, F., Staubwasser, M., Schneider, R.R., Steig, E.J., 2004. Holocene climate variability. Quat. Res. 62 (3), 243–255. https://doi.org/10.1016/j.yqres.2004.07.001.

Móga, J., Kiss, K., Borsodi, A., Szabó, M., Strat, D., Barbara, B., 2018. The analysis of relationship between microclimate and microbial carbon-dioxide production in the soils of the Tapolca and Gömör-Tornai karst terrains. Hungary. 17 (1).

Moossen, H., Bendle, J., Seki, O., Quillmann, U., Kawamura, K., 2015. North Atlantic Holocene climate evolution recorded by high-resolution terrestrial and marine biomarker records. Quat. Sci. Rev. 129, 111–127. https://doi.org/10.1016/j.quascirev.2015.10.013.

Orbán, I., Birks, H.H., Vincze, I., Finsinger, W., Pál, I., Marinova, E., Jakab, G., Braun, M., Hubay, K., Bíró, T., 2018. Treeline and timberline dynamics on the northern and southern slopes of the Retezat Mountains (Romania) during the late glacial and the Holocene. Quat. Int. 477, 59–78.

Orme, L.C., Miettinen, A., Seidenkrantz, M.-S., Tuominen, K., Pearce, C., Divine, D.V., Oksman, M., Kuijpers, A., 2021. Mid to late-Holocene Sea-surface temperature variability off north-eastern Newfoundland and its linkage to the North Atlantic Oscillation. The Holocene 31 (1), 3–15. https://doi.org/10.1177/0959683620961488.

Pálfi, I., Pósfai, M., Kristály, F., Veres, D., Arnaud, F., Szalai, Z., Magyari, E., 2021. Geochexment and paleoclimate. In: EGU General Assembly Conference Abstracts. EGU21-15654, April.

Perşoiu, A., Onac, B.P., Wynn, J.G., Blaauw, M., Ionita, M., Hansson, M., 2017. Holocene winter climate variability in Central and Eastern Europe. Sci. Rep. 7 (1), 1196. https://doi.org/10.1038/s41598-017-01397-w.

Peyron, O., Goring, S., Dormoy, I., Kotthoff, U., Pross, J., de Beaulieu, J.-L., Drescher-Schneider, R., Vannière, B., Magny, M., 2011. Holocene seasonality changes in the Central Mediterranean region reconstructed from the pollen sequences of Lake Accesa (Italy) and Tenaghi Philippon (Greece). The Holocene 21 (1), 131–146. https://doi.org/10.1177/0959683610384162.

Peyron, O., Magny, M., Goring, S., Joannin, S., de Beaulieu, J.-L., Brugiapaglia, E., Sadori, L., Garfi, G., Kouli, K., Ioakim, C., Combourieu-Nebout, N., 2013. Contrasting patterns of climatic changes during the Holocene across the Italian Peninsula reconstructed from pollen data. Clim. Past 9 (3), 1233–1252. https://doi.org/10.5194/cp-9-1233-2013.

Peyron, O., Combourieu-Nebout, N., Brayshaw, D., Goring, S., Andrieu-Ponel, V., Desprat, S., Fletcher, W., Gambin, B., Ioakim, C., Joannin, S., Kotthoff, U., Kouli, K., Montade, V., Pross, J., Sadori, L., Magny, M., 2017. Precipitation changes in the Mediterranean basin during the Holocene from terrestrial and marine pollen records: a model–data comparison. Clim. Past 13 (3), 249–265. https://doi.org/10.5194/cp-13-249-2017.

R Development Core Team, 2015. R: A Language and Environment for Statistical Computing. R Foundation for Statistical Computing, Vienna.

Raberg, J.H., Harning, D.J., Crump, S.E., de Wet, G., Blumm, A., Kopf, S., Geirsdóttir, Á., Miller, G.H., Sepúlveda, J., 2021. Revised fractional abundances and warm-season temperatures substantially improve brGDGT calibrations in lake sediments. Biogeosciences 18 (12), 3579–3603. https://doi.org/10.5194/bg-18-3579-2021.

Ramos-Román, M.J., Jiménez-Moreno, G., Camuera, J., García-Alix, A., Scott Anderson, R., Jiménez-Espejo, F.J., Sachse, D., Toney, J.L., Carrión, J.S., Webster, C., Yanes, Y., 2018. Millennial-scale cyclical environment and climate variability during the Holocene in the western Mediterranean region deduced from a new multi-proxy analysis from the Padul record (Sierra Nevada, Spain). Glob. Planet. Chang. 168, 35–53. https://doi.org/10.1016/j.gloplacha.2018.06.003.

Ran, M., Chen, L., 2019. The 4.2 ka BP climatic event and its cultural responses. Quat. Int. 521, 158–167. https://doi.org/10.1016/j.quaint.2019.05.030.

Rasmussen, T.L., Thomsen, E., Moros, M., 2016. North Atlantic warming during Dansgaard-Oeschger events synchronous with Antarctic warming and out-of-phase with Greenland climate. Sci. Rep. 6, 20535. PMC. https://doi.org/10.1038/srep20535.

Reimer, P.J., Austin, W.E., Bard, E., Bayliss, A., Blackwell, P.G., Ramsey, C.B., Butzin, M., Cheng, H., Edwards, R.L., Friedrich, M., 2020. The IntCal20 Northern Hemisphere radiocarbon age calibration curve (0–55 cal kBP). Radiocarbon 62 (4), 725–757.

Renssen, H., Seppa, H., Heiri, O., Roche, D.M., Goosse, H., Fichefet, T., 2009. The spatial and temporal complexity of the Holocene thermal maximum. Nat. Geosci. 2 (6), 411–414. https://doi.org/10.1038/ngeo513.

Schnitchen, C., Charman, D.J., Magyari, E., Braun, M., Grigorszky, I., Tóthmérész, B., Molnár, M., Szántó, Z., 2006. Reconstructing hydrological variability from testate amoebae analysis in Carpathian peatlands. J. Paleolimnol. 36 (1), 1–17.

Schöll-Barna, G., Demény, A., Serlegi, G., Fábián, S., Sümegi, P., Fóris, I., Bajnóczi, B., 2012. Climatic variability in the Late Copper Age: Stable isotope fluctuation of prehistoric Unio pictorum (Unionidae) shells from Lake Balaton (Hungary). J. Paleolimnol. 47 (1), 87–100.

Sicre, M.-A., Jalali, B., Eiríksson, J., Knudsen, K.-L., Klein, V., Pellichero, V., 2021. Trends and centennial-scale variability of surface water temperatures in the North Atlantic during the Holocene. Quat. Sci. Rev. 265, 107033 https://doi.org/10.1016/j.quascirev.2021.107033.

Sinninghe Damsté, J.S., Hopmans, E.C., Pancost, R.D., Schouten, S., Geenevasen, J.A.J., 2000. Newly discovered non-isoprenoid glycerol dialkyl glycerol tetraether lipids in sediments. Chem. Commun. 17, 1683–1684. Scopus.

Strat, D., 2016. Floristic composition and functional zones pattern of the beach-dune system along the Danube Delta coast - Romania. Forum geografic XV (1), 65–79. https://doi.org/10.5775/fg.2016.093.i.

Tantau, I., Reille, M., de Beaulieu, J.-L., Farcas, S., 2006. Late Glacial and Holocene vegetation history in the southern part of Transylvania (Romania): Pollen analysis of two sequences from Avrig. J. Quat. Sci. 21 (1), 49–61. https://doi.org/10.1002/jqs.937.

Tantau, I., Reille, M., de Beaulieu, J.-L., Farcas, S., Goslar, T., Paterne, M., 2003. Vegetation history in the Eastern Romanian Carpathians: pollen analysis of two sequences from the Mohoş crater. Vegetation Hist. Archaeobot. 12, 113–125. https://doi.org/10.1007/s00334-003-0015-6.

Tarroso, P., Carrión, J., Dorado-Valiño, M., Queiroz, P., Santos, L., Valdeolmillos-Rodríguez, A., Célio Alves, P., Brito, J.C., Cheddadi, R., 2016. Spatial climate dynamics in the Iberian Peninsula since 15 000 yr BP. Clim. Past 12 (5), 1137–1149. https://doi.org/10.5194/cp-12-1137-2016.

ter Braak, C.J.F., Juggins, S., 1993. Weighted averaging partial least squares regression (WA-PLS): An improved method for reconstructing environmental variables from species assemblages. In: van Dam, H. (Ed.), Twelfth International Diatom Symposium. Springer, Netherlands, pp. 485–502.

Tierney, J.E., Russell, J.M., 2009. Distributions of branched GDGTs in a tropical lake system: implications for lacustrine application of the MBT/CBT paleoproxy. Org. Geochem. 40 (9), 1032–1036. https://doi.org/10.1016/j.orggeochem.2009.04.014.

Tóth, M., Magyari, E.K., Buczkó, K., Braun, M., Panagiotopoulos, K., Heiri, O., 2015. Chironomid-inferred Holocene temperature changes in the South Carpathians (Romania). The Holocene 25 (4), 569–582. https://doi.org/10.1177/0959683614565953.

Túri, M., Hubay, K., Molnár, M., Braun, M., László, E., Futó, I., Palcsu, L., 2021. Holocene paleoclimate inferred from stable isotope (δ18O and δ13C) values in Sphagnum cellulose, Mohos peat bog, Romania. J. Paleolimnol. 1–20.

Vincze, I., Finsinger, W., Jakab, G., Braun, M., Hubay, K., Veres, D., Deli, T., Szalai, Z., Szabó, Z., Magyari, E., 2019. Paleoclimate reconstruction and mire development in the Eastern Great Hungarian Plain for the last 20,000 years. Rev. Palaeobot. Palynol. 271, 104112. https://doi.org/10.1016/j.revpalbo.2019.104112.

Vincze, I., Orbán, I., Birks, H.H., Pál, I., Finsinger, W., Hubay, K., Marinova, E., Jakab, G., Braun, M., Bíró, T., Tóth, M., Dänäu, C., Ferencz, I.V., Magyari, E.K., 2019. Holocene treeline and timberline changes in the South Carpathians (Romania): Climatic and anthropogenic drivers on the southern slopes of the Retezat Mountains. The Holocene 27 (11), 1613–1630. https://doi.org/10.1177/0959683617702227.

Walker, M.J.C., Berkelhammer, M., Björck, S., Cwynar, L.C., Fisher, D.A., Long, A.J., Lowe, J.J., Newnham, R.M., Rasmussen, S.O., Weiss, H., 2012. Formal subdivision of

the Holocene Series/Epoch: a Discussion Paper by a Working Group of INTIMATE (Integration of ice-core, marine and terrestrial records) and the Subcommission on Quaternary Stratigraphy (International Commission on Stratigraphy). J. Quat. Sci. 27 (7), 649–659. https://doi.org/10.1002/jqs.2565.

Wanner, H., Mercolli, L., Grosjean, M., Ritz, S., 2015. Holocene climate variability and change; a data-based review. J. Geol. Soc. 172 (2), 254–263.

Weijers, J.W.H., Schouten, S., Hopmans, E.C., Geenevasen, J.A.J., David, O.R.P., Coleman, J.M., Pancost, R.D., Sinninghe Damsté, J.S., 2006. Membrane lipids of mesophilic anaerobic bacteria thriving in peats have typical archaeal traits. Environ. Microbiol. 8 (4), 648–657. https://doi.org/10.1111/j.1462-2920.2005.00941.x.

Weber, Y., Sinninghe Damsté Jaap, S., Zopfi, J., De Jonge, C., Gilli, A., Schubert Carsten, J., Lepori, F., Lehmann Moritz, F., Niemann, H., 2018. Redox-dependent niche differentiation provides evidence for multiple bacterial sources of glycerol

tetraether lipids in lakes. Proceed. Nat. Acad. Sci. 115, 10926–10931. https://doi.org/10.1073/pnas.1805186115.

Weijers, J.W.H., Schefuß, E., Schouten, S., Sinninghe Damsté, J.S.S., 2007. Coupled thermal and hydrological evolution of tropical africa over the last deglaciation. Science 315 (5819), 1701. https://doi.org/10.1126/science.1138131.

Xiao, W., Wang, Y., Zhou, S., Hu, L., Yang, H., Xu, Y., 2016. Ubiquitous production of branched glycerol dialkyl glycerol tetraethers (brGDGTs) in global marine environments: a new source indicator for brGDGTs. Biogeosciences 13 (20), 5883–5894. https://doi.org/10.5194/bg-13-5883-2016.

Zielhofer, C., Fletcher, W.J., Mischke, S., De Batist, M., Campbell, J.F.E., Joannin, S., Tjallingii, R., El Hamouti, N., Junginger, A., Stele, A., Bussmann, J., Schneider, B., Lauer, T., Spitzer, K., Strupler, M., Brachert, T., Mikdad, A., 2017. Atlantic forcing of Western Mediterranean winter rain minima during the last 12,000 years. Quat. Sci. Rev. 157 (Supplement C), 29–51. https://doi.org/10.1016/j.quascirev.2016.11.037.